



Labyrinthine Pattern Formation in Magnetic Fluids

Akiva J. Dickstein; Shyamsunder Erramilli; Raymond E. Goldstein; David P. Jackson;
Stephen A. Langer

Science, New Series, Vol. 261, No. 5124 (Aug. 20, 1993), 1012-1015.

Stable URL:

<http://links.jstor.org/sici?sici=0036-8075%2819930820%293%3A261%3A5124%3C1012%3ALPFIMF%3E2.0.CO%3B2-F>

Science is currently published by American Association for the Advancement of Science.

Your use of the JSTOR archive indicates your acceptance of JSTOR's Terms and Conditions of Use, available at <http://www.jstor.org/about/terms.html>. JSTOR's Terms and Conditions of Use provides, in part, that unless you have obtained prior permission, you may not download an entire issue of a journal or multiple copies of articles, and you may use content in the JSTOR archive only for your personal, non-commercial use.

Please contact the publisher regarding any further use of this work. Publisher contact information may be obtained at <http://www.jstor.org/journals/aaas.html>.

Each copy of any part of a JSTOR transmission must contain the same copyright notice that appears on the screen or printed page of such transmission.

JSTOR is an independent not-for-profit organization dedicated to creating and preserving a digital archive of scholarly journals. For more information regarding JSTOR, please contact support@jstor.org.

132. D. Weigent, J. Blalock, R. LeBoeuf, *Endocrinology* **128**, 2053 (1991).
133. A. Brunetti *et al.*, *J. Biol. Chem.* **265**, 13435 (1990).
134. F. Cope, J. Wille, L. D. Tomei, in (77), pp. 125–142.
135. F. Cope and J. Wille, *Proc. Natl. Acad. Sci. U.S.A.* **86**, 5590 (1989).
136. A. Ao *et al.*, *Antisense Res. Dev.* **1**, 1 (1991).
137. A. Caceres, S. Potrebic, K. Kosik, *J. Neurosci.* **11**, 1515 (1991).
138. E. Sorscher *et al.*, *Proc. Natl. Acad. Sci. U.S.A.* **88**, 7759 (1991).
139. M. Listerud, A. Brussaard, P. Devay, D. Colman, L. Role, *Science* **254**, 1518 (1991).
140. M. Clark *et al.*, *Proc. Natl. Acad. Sci. U.S.A.* **88**, 5418 (1991).
141. A. Teichman-Weinber, U. Z. Littauer, I. Ginzburg *Gene* **72**, 297 (1988).
142. M. Shoemaker *et al.*, *J. Cell Biol.* **111**, 1107 (1990).
143. G. Thinakaran and J. Bag, *Exp. Cell Res.* **192**, 227 (1991).
144. R. Pepperkok *et al.*, *ibid.* **197**, 245 (1991).
145. L. Bavisotto *et al.*, *J. Exp. Med.* **174**, 1097 (1991).
146. P. Porcu *et al.*, *Mol. Cell. Biol.* **12**, 5069 (1992).
147. L. Neyses, J. Nuskas, H. Vetter, *Biochem. Biophys. Res. Commun.* **181**, 22 (1991).
148. M. Kanbe *et al.*, *Anti-Cancer Drug Des.* **7**, 341 (1992).
149. J. Cook *et al.*, *Antisense Res. Dev.* **2**, 199 (1992).
150. A. West and B. Cooke, *Mol. Cell. Endocrinol.* **79**, R9 (1991).
151. A. Witsell and L. Schook, *Proc. Natl. Acad. Sci. U.S.A.* **89**, 4754 (1992).
152. C.A.S. is the Irving Assistant Professor of Medicine and Pharmacology at Columbia University and is grateful to the Mathieson Foundation and the Dubose Hayward Foundation for support. A. Krieg, J. Reed, and M. Caruthers participated in helpful conversations. The research of Y.-C.C. is supported by a grant from the National Cancer Institute (CA 44538).

RESEARCH ARTICLE

Labyrinthine Pattern Formation in Magnetic Fluids

Akiva J. Dickstein, Shyamsunder Erramilli, Raymond E. Goldstein,*
David P. Jackson, Stephen A. Langer

A quasi two-dimensional drop of a magnetic fluid (ferrofluid) in a magnetic field is one example of the many systems, including amphiphilic monolayers, thin magnetic films, and type I superconductors, that form labyrinthine patterns. The formation of the ferrofluid labyrinth was examined both experimentally and theoretically. Labyrinth formation was found to be sensitively dependent on initial conditions, indicative of a space of configurations having a vast number of local energy minima. Certain geometric characteristics of the labyrinths suggest that these multiple minima have nearly equivalent energies. Kinetic effects on pattern selection were found in studies of fingering in the presence of time-dependent magnetic fields. The dynamics of this pattern formation was studied within a simple model that yields shape evolutions in qualitative agreement with experiment.

Several distinct physical systems form strikingly similar labyrinthine structures. These include thin magnetic films (1, 2), amphiphilic "Langmuir" monolayers (3–5), and type I superconductors in magnetic fields (6). Similarities between the energetics of these systems suggest a common mechanism for pattern formation. In each case, the labyrinth is formed by the boundary between two thermodynamic phases (oppositely magnetized domains, expanded and condensed dipolar phases, or normal and superconducting regions), and has an associated surface tension favoring a minimum interface length. Each also has long-range dipolar interactions. These may be

electrostatic, as in amphiphilic monolayers (the dipolar molecules of which are perpendicular to the air-water interface), or may be due to bulk magnetization (permanent or induced, as in superconductors). These interactions are repulsive, favoring an extended interface. From a dynamical point of view, the evolution of each of the patterns in the presence of a global constraint such as prescribed magnetization, constant domain area, or fixed magnetic flux, respectively. In each case, the shape evolution is also dominated by dissipation.

It has been recognized for some time, both in the context of amphiphilic systems (7) and superconductors (8), that the competition between long-range forces and surface tension can result in a variety of regular patterns such as lamellar stripe domains and hexagonal arrays. The more widely encountered irregular, or disordered, patterns are poorly understood. In analyzing these shapes, a number of general questions naturally arise. (i) Is an observed time-inde-

pendent shape a unique energetic ground state or does the energy functional contain multiple minima? (ii) If the latter, are the minima roughly equivalent in energy? (iii) Might kinetic considerations force a relaxing system into a metastable minimum instead of the true ground state? Such questions are of course not confined to these particular examples of pattern formation, but also arise in systems such as spin glasses (9) and protein folding (10).

Motivated by the above-mentioned similarities among labyrinthine pattern forming systems, we have investigated the fingering instabilities of macroscopic domains of magnetic fluids (also known as "ferrofluids"), which are colloidal suspensions of microscopic magnetic particles in a hydrocarbon medium (11). Ferrofluids are known to produce complex labyrinthine patterns when trapped between closely spaced glass plates (a "Hele-Shaw cell") and subjected to a magnetic field normal to the plates (11–13). Here, as in the systems described above, there is a competition between the ferrofluid-water surface tension and bulk induced magnetic dipole interactions. The motion satisfies a global constraint (fixed fluid volume) and is dominated by viscosity. The macroscopic nature of this system affords distinct experimental advantages, including ease of visualization and direct con-

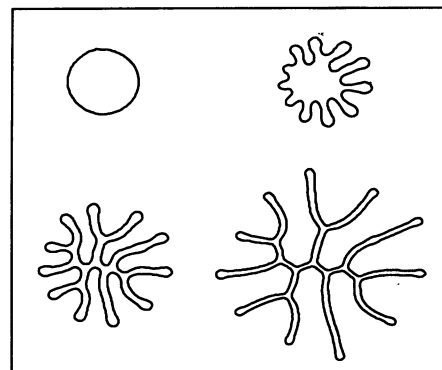


Fig. 1. Stages in the fingering instability of a magnetic fluid drop of initial diameter 2.1 cm, in a field of 87 gauss, as seen from above.

A. J. Dickstein, S. Erramilli, R. E. Goldstein, and D. P. Jackson are in the Department of Physics, Joseph Henry Laboratories, Princeton University, Princeton, NJ 08544. S. Erramilli and R. E. Goldstein are also affiliated with the Princeton Materials Institute, Bowen Hall, Princeton University, Princeton, NJ 08540. S. A. Langer is in the Department of Physics, Simon Fraser University, Burnaby, British Columbia, V5A 1S6, Canada.

*To whom correspondence should be addressed.

trol of the strength of dipolar interactions.

Our focus is on the shape evolution of circular domains made unstable by the application of a magnetic field. These experiments are complementary to recent studies of dipolar shape relaxation in amphiphilic monolayers (14). We obtained experimental answers to the three questions raised above and describe here theoretical models (15, 16) that reproduce the essential qualitative features of the experiments.

Existence of multiple minima. The experimental apparatus (17) was similar to that already described (18). Snapshots of the time evolution of a drop undergoing a fingering instability are shown in Fig. 1. We see the initial instability of the circular shape evolve quickly to a well-defined branched structure (a “tree”) that then spreads without any further change in connectivity. Ramping the field slowly back to zero restored the shapes to their original circular form, although rapid quenching sometimes resulted in fission into droplets. The variability of the patterns from one run to the next is illustrated in Fig. 2, which shows shapes produced by ramps to low and high fields. These ramps generally were accomplished in 1 second. The patterns are the results of evolutions lasting for approximately 60 to 150 second after the application of the field. The local stability of these patterns was tested by superimposing on the dc magnetic field a small sinusoidal field. While this perturbed the arm positions and shape, the tree returned to its original shape when the oscillating field was removed.

The final trees differed in the shapes, lengths, and connectivity of their branches (19). All observed trees had n free ends and $n - 2$ threefold coordinated nodes, at

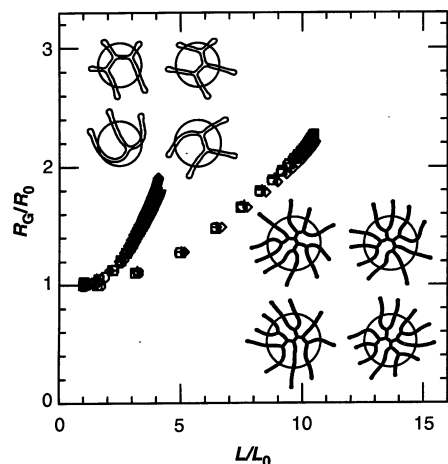


Fig. 2. Final states obtained at for two drop radii and field strengths (upper left) $R_0 = 0.55$ cm, $H = 75$ gauss; (lower right) $R_0 = 1.1$ cm, $H = 87$ gauss. Circles indicate radii of gyration. Paths in the space of perimeter (L) and radius of gyration (R_G), normalized by the values for the initial circle, showing high degree of overlap.

which branches met at nearly 120° . They may be classified according to their “topology,” the particular connectivity of the nodes. We have observed all possible distinct topologies for $n \leq 7$, and many topologies for larger n .

Equivalence of multiple minima. As is apparent from the branched patterns in Fig. 2, even within a given topology there was variability of the details of the shape. Nevertheless, the trees formed under given experimental conditions (ramp rate and final field value) yielded similar values for two very basic geometric quantities: the perimeter L and radius of gyration R_G , defined as $R_G^2 \equiv (1/L) \oint ds [\mathbf{r}(s) - \mathbf{r}_c]^2$. Here $\mathbf{r}(s)$ is the boundary of the pattern, s is arc length, and $\mathbf{r}_c \equiv (1/L) \oint ds \mathbf{r}(s)$ is the center of mass of the boundary. A convenient method for summarizing the shape evolution is to consider its trajectory in the $L - R_G$ plane, with time varying parametrically (Fig. 2). Evidently, patterns which differ in the details of their branching may nevertheless exhibit a high degree of overlap, both during the evolution and in their final states. We suggest below that this overlap indicates that these patterns have nearly equivalent energies.

Kinetic effects. We found that the degree of branching of the initially circular shape depended not only on the magnitude of the applied magnetic field, but also on the rate at which that field was ramped to its final value. This pattern selection may be quantified by determining the wavelength λ of the initial instability by examining videotaped images just after the onset of the ramp. Although, as a result of tip-splitting or competition between branches, the stationary long-time tree and the initial instability may differ in the number of their branches, the initial instability is more likely to be understandable within a linear or weakly nonlinear analysis. The initial mode number $n = L_0/\lambda$ depended on the field ramp rate $\alpha \equiv dH/dt$, as α varied over three orders of magnitude (Fig. 3). An approximate power-law behavior, $n \approx (dH/dt)^\psi$ is shown in the inset, along with the prediction $\psi \approx 0.25$, arising from the theory described below. The selection occurred long before the ramping was complete.

Energetics. A theory for this pattern formation must address both the energetics and the dynamics of labyrinthine structures. In designing the simplest model, we assume that the magnetization $\mathbf{M} = M\hat{\mathbf{z}}$ within the domain is uniform (20), but account for the energy associated with the demagnetizing field, so the magnetic energy is just that of two sheets of opposite charge density $\sigma = \mathbf{M} \cdot \hat{\mathbf{z}}$, separated by a height h in the z direction, and bounded by the curve $\mathbf{r}(s)$ in the xy plane. It is thus equivalent in form to the energy of a parallel plate capac-

itor, a model used to describe dipolar amphiphilic domains. The field energy may be expressed (15) as a pair interaction between the local unit tangent vectors $\hat{\mathbf{t}}(s)$ of the curve. Apart from a term proportional to the slab volume, the total energy is $\mathcal{E}_0[\mathbf{r}] =$

$$\gamma L - M^2 h \oint ds \oint ds' \hat{\mathbf{t}}(s) \cdot \hat{\mathbf{t}}(s') \Phi(R/h) \quad (1)$$

where γ is the line tension, $R = |\mathbf{R}| = |\mathbf{r}(s) - \mathbf{r}(s')|$, and $\Phi(\xi) = \sinh^{-1}(1/\xi) + \xi - \sqrt{1 + \xi^2}$. The somewhat complicated function $\Phi(R/h)$, arising from integrations over the thickness of the slab, decays like $1/R$ at large R , but crosses over to $-\ln R$ at small R , preventing divergences in the integral and obviating the need for additional small scale cutoffs (21). The form of the magnetic interaction in Eq. 1 is to be anticipated from the usual association between magnetic moments and current loops, the scalar product reflecting the attraction (repulsion) between parallel (antiparallel) current-carrying wires.

Just as the existence of long-range forces in fluids justifies mean or molecular field theories, we expect the magnetic energy to be less sensitive to details of the spatial arrangement of the interface than to the overall scale of the pattern, given by R_G . The surface energy naturally scales with the perimeter L , so different experimentally observed shapes with similar L and R_G are likely to be similar in energy.

Turning now to the details of the branched patterns, we find a convenient dimensionless measure of the relative strength of dipolar and surface energies is the Bond number (11)

$$N_{Bo} = 2M^2 h^2 / \gamma \quad (2)$$

When N_{Bo} is small, line tension dominates, and the droplets will be circular. When N_{Bo}

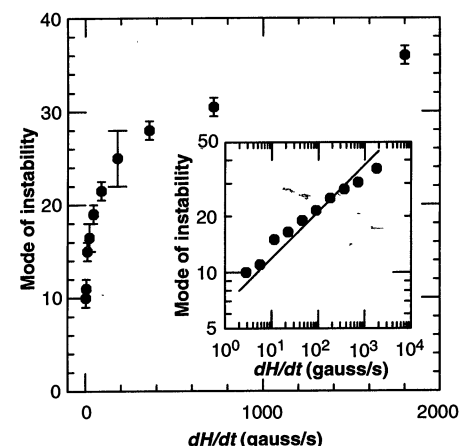


Fig. 3. Initial mode of instability n as a function of magnetic field ramp rate, for quenches of a 4.9-cm (diameter) circular drop to 265 gauss. Inset shows data on a log-log plot. The slope of the line is $1/4$, as shown in Eq. 14.

is large, dipole forces dominate, and labyrinthine patterns develop. The Bond number for electric dipole systems with dipole density μ per unit area is obtained by substituting $\mu = Mh$ in Eq. 2.

To understand the well-defined arm width seen in the experimental patterns, consider a long, thin, rectangular stripe of width $w > h$, length $\ell \gg w$, and conserved area $A = w\ell$. If we ignore end contributions, the surface energy of the stripe is $2\gamma\ell$. To estimate its magnetic energy, we focus on the scaling properties of the double integral in Eq. 1, approximating the function $\Phi(\xi)$ by $1/2\xi$ for $\xi > 1$ and $1/2$ for $0 < \xi < 1$. Recognizing that w replaces h as the cutoff for interactions on opposite sides, we obtain the estimate

$$\mathcal{E}_0 \sim 2\gamma\ell + 2M^2h^2\ell[\ln(h/w) - 1] \quad (3)$$

Minimizing with respect to w at fixed A , and considering the limit $h^2/A \ll 1$, we find the equilibrium width

$$w \sim he^{2/N_{Bo}} \quad (4)$$

Thus the width decreases with increasing field, as is indeed the case in experiment (Fig. 2). The observed threefold coordination of the nodes in the pattern arises from the interplay of the repulsion of the arms and surface tension effects. A fourfold node is unstable to the creation of two threefold nodes with internal angles of 120° .

Dynamics. At the ferrofluid-water interface the force that leads to shape relaxation is the pressure difference $\Delta\Pi$ arising from the line tension and magnetic interactions. That pressure is related to the energy \mathcal{E} via

$$\Delta\Pi = -\hat{n} \cdot \frac{\delta\mathcal{E}}{\delta\mathbf{r}} \quad (5)$$

\hat{n} is the unit outward normal to the interface. The simplest dynamical model (15) for the pattern formation is that the shape follows the path of steepest descent of its energy: a "gradient flow" in configuration space. Here, the dissipation is taken to be local (as one might find for domain wall motion in solid-state systems), and

$$\hat{n} \cdot \frac{\partial\mathbf{r}}{\partial t} = \tilde{\Gamma}\Delta\Pi = -\tilde{\Gamma}\hat{n} \cdot \frac{\delta\mathcal{E}}{\delta\mathbf{r}} \quad (6)$$

where $\tilde{\Gamma}$ is a kinetic coefficient. The constraint of constant enclosed area is enforced with a Lagrange multiplier p by using a Legendre-transformed energy $\mathcal{E} = \mathcal{E}_0 - pA$ in Eq. 6. The resulting equation of motion for this "dissipative dynamics" is

$$\hat{n} \cdot \frac{\partial\mathbf{r}}{\partial t} = -\gamma\kappa + 2M^2\phi ds' \hat{\mathbf{R}} \times \hat{\mathbf{t}}(s') \\ \times \left[\sqrt{1 + (h/R)^2} - 1 \right] + p[\mathbf{r}(s)] \quad (7)$$

where $\kappa(s)$ is the curvature, $\hat{\mathbf{R}} = \mathbf{R}/R$, and $p[\mathbf{r}]$ is determined by $dA/dt = 0$. The first term in Eq. 7 is the familiar Laplace pres-

sure across a curved interface, while the second is the Biot-Savart contribution from a current ribbon of finite height h .

A more realistic description of the hydrodynamics in the Hele-Shaw cell accounts for the entire flow field through Darcy's law (22), which gives the fluid velocity \mathbf{v} in terms of gradients of the total pressure Π ,

$$\mathbf{v} = -\Gamma\nabla\Pi \quad (8)$$

Here, $\Gamma = h^2/12\eta$, and η is the fluid viscosity. This law of motion, also applicable to flow in porous media, may be derived by neglecting the inertial terms in the Navier Stokes equation and assuming that the dissipation is dominated by viscous interactions with the plates. The velocity \mathbf{v} in Eq. 8 is a two-dimensional, z -averaged quantity, and the pressure jump in Eq. 5 becomes a boundary condition applied at the ferrofluid-water interface. Area conservation is automatically obtained from the incompressibility of the flow (23).

These two approaches to the interface evolution are complementary; the first, in focusing on the forces and ignoring the nonlocality associated with the fluid incompressibility, is computationally simpler, while the second is more faithful to the hydrodynamics but computationally intensive. We have studied both in detail and find their predictions to be qualitatively similar, although quantitatively distinct.

Insight into the basic mechanism of the fingering instability comes from a linear stability analysis of a circle of radius R_0 (12, 15), particularly in the limit of large aspect ratio, $R_0/h \gg 1$, which is the case for our experiments. A perturbation of the radius of the circle in the form $\zeta_n(t)\cos(n\theta)$ evolves as $\partial\zeta_n/\partial t = \sigma_n\zeta_n$, where the growth rate σ_n in Hele-Shaw flow is given for small n by

$$\sigma_n \approx \frac{\Gamma}{R_0^3} n \left[\tilde{\gamma}(1 - n^2) - M^2h^2n^2\ln(n) \right] \quad (9)$$

The result from dissipative dynamics differs only in the absence of an overall factor of n/R_0 , reflecting the additional gradient in Eq. 8. Here, the effective line tension is

$$\tilde{\gamma} = \gamma - M^2h^2[1 - C + \ln(2R_0/h)] \quad (10)$$

where C is Euler's constant. Equations 9 and 10 show that, as the magnetic field (or aspect ratio) is increased, the circle becomes unstable ($\sigma_n > 0$) due to an effective negative line tension while the magnetic forces stabilize the short-wavelength modes. Within this approximation, the fastest growing mode n^* is given by

$$n^* \sim \frac{R_0}{h} e^{-2/N_{Bo}} \quad (11)$$

increasing with increasing field.

A qualitative explanation for the mode

selection in the ramping experiments follows from these results. Let us suppose that the field is linear in time, as in our experiments: $H = \alpha t$. Then, for fields below the saturation magnetization, M will also be linear: $M = \chi\alpha t$, where χ is the susceptibility. From Eq. 11, at different times different modes will be growing fastest, and the mode which is observed at long times will be the mode which was growing fast enough and long enough to acquire a sufficient amplitude to suppress the other modes. If the ramp is slow, low-order modes grow large before higher ones become unstable, and the pattern has few branches. In a fast ramp, the low modes have not had time to grow before higher modes, with faster growth rates, become unstable and overtake them.

When the wavelength of a mode is small compared to the perimeter of the circle, and the magnetization has the above-mentioned time dependence, we find that the dispersion relation is well approximated by the form

$$\sigma_n(t) \approx \frac{\Gamma}{R_0^3} \left[(\chi\alpha t)^2 \frac{n}{R_0} - \gamma \left(\frac{n}{R_0} \right)^3 \right] \quad (12)$$

If there were no explicit time dependence to σ , it would be plausible to postulate that the fastest-growing mode would be selected. With time dependence, however, we claim that mode selection occurs through nonlinear effects when the amplitudes reach some threshold value. The time τ_n required for the n th mode to reach the threshold is given by

$$\frac{\zeta_n(\tau_n)}{\zeta_n(0)} = \exp \left[\int_0^{\tau_n} dt \sigma_n(t) \right] = \text{constant} \quad (13)$$

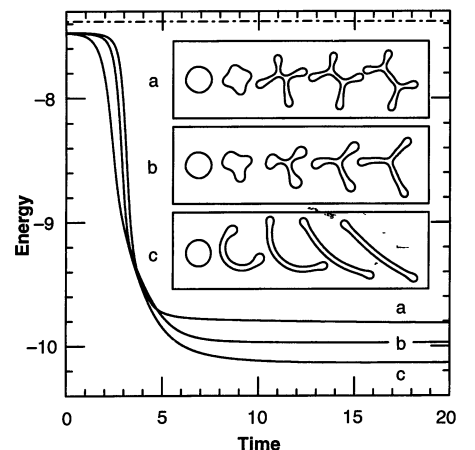


Fig. 4. Shape evolution and energy relaxation from the dissipative dynamics formalism, for $N_{Bo} = 1.12$ and $R_0/h = 10.0$. Dashed line indicates the energy of a perfect circle, solid lines are for three initial conditions weakly perturbed from a circle. The unbranched structure lies lower in energy.

The selected mode n^* will be the one with the smallest τ_n . From Eqs. 12 and 13, we find that n^* scales as a power of the ramp rate α ,

$$n^* \sim \alpha^{1/4} \quad (14)$$

in fair agreement with the data (see Fig. 3).

The linear analysis is of limited predictive ability regarding the final state. At present, an understanding of the nonlinear regime requires numerical study. The models described above allow us to study branch competition near the linear regime, as well as to compare the energies of the patterns obtained at long times. Figure 4 shows three evolutions from nearby initial conditions obtained with the use of the dissipative dynamics in Eq. 7. We see that the unbranched tree lies lowest in energy, and that there is apparently a "vertex energy" associated with each threefold coordinated node.

The fingering of several branched structures obtained from a conformal mapping approach (16, 24) to the Hele-Shaw dynamics is shown in Fig. 5. The overall structure is in good qualitative accord with the experimental patterns, displaying a well-defined finger width and the proper internal node structure. We do not expect nonuniformities in the magnetization to make qualitative changes to the pattern formation although there may be quantitative effects, such as a lowering of the energy below that estimated in Eq. 1. An understanding of these effects remains, however, an open problem. The dynamics also displays sensitive dependence on initial conditions, in the sense that nearly identical starting configurations (circles perturbed slightly by different sets of modes ζ_n) can lead to vastly different final states. These initial conditions can arise experimentally as a consequence of thermal fluctuations or material inhomogeneities. The precise connection between these initial perturbations and the final branched structures is not completely understood. In accord with experiment we find that fourfold vertices are unstable toward vertex fission, creating two threefold vertices. This process bears a resemblance to topology transitions in soap froths (25). In numerical simulations, it is often extremely difficult to distinguish between true local minima and very shallow slopes of the energy functional in the configuration space. Thus, we cannot rule out the possibility that the experimentally ob-

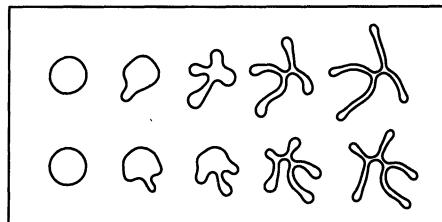


Fig. 5. The theoretical shape evolutions obtained from conformal mapping solution to Darcy's law dynamics for magnetic fluids. Both sequences are for $R_0/h = 10.0$ and $N_{Bo} = 1.20$. The top resulted from a ramp in N_{Bo} , while the bottom followed an instantaneous jump of the Bond number.

served patterns are not true local minima, but are made locally stable by stick-slip friction against the plates in the Hele-Shaw cell or other effects not accounted for within Darcy's law.

In conclusion, the branched patterns seen in experiment can be understood within perhaps the simplest dynamical models incorporating the competition between surface and dipolar energies. Taken together, the experimental and theoretical results indicate that an enormously complex energy landscape in the space of shapes can arise from a competition between short-range forces and long-range dipolar interactions in systems subject to a geometric constraint. A static theory of labyrinths would find only the minimum energy configurations, whereas the dynamic theories reflect the complexity of the landscape in the complexity of the labyrinths.

REFERENCES AND NOTES

1. M. Seul, L. R. Monar, L. O'Gorman, R. Wolfe, *Science* **254**, 1616 (1991).
2. P. Molho, J. L. Porteseil, Y. Souche, J. Gouzerh, J. C. S. Levy, *J. Appl. Phys.* **61**, 4188 (1987).
3. H. Möhwald, *Annu. Rev. Phys. Chem.* **41**, 441 (1990), and references therein.
4. H. M. McConnell, *ibid.* **42**, 171 (1991), and references therein.
5. M. Seul and M. J. Sammon, *Phys. Rev. Lett.* **64**, 1903 (1990); M. Seul, *Physica A* **168**, 198 (1990).
6. F. Haenssler and L. Rinderer, *Helv. Phys. Acta* **40**, 659 (1967); R. P. Huebner, *Magnetic Flux Structures in Superconductors* (Springer-Verlag, New York, 1979).
7. D. Andelman, F. Brochard, J.-F. Joanny, *J. Chem. Phys.* **86**, 3673 (1987).
8. L. D. Landau, *Zh. Eksp. Teor. Fiz.* **7**, 371 (1937).
9. K. Binder and A. Young, *Rev. Mod. Phys.* **58**, 846 (1986).
10. H. Frauenfelder, S. G. Sligar, P. G. Wolynes, *Science* **254**, 1598 (1991), and references therein.
11. R. E. Rosensweig, *Ferrohydrodynamics* (Cambridge Univ. Press, Cambridge, 1985).
12. A. O. Tsebers and M. M. Maiorov, *Magneto-hydrodynamics* **16**, 21 (1980).
13. A. G. Boudouvis, J. L. Puchalla, L. E. Scriven, *J. Coll. Int. Sci.* **124**, 688 (1988).
14. M. Seul, *J. Phys. Chem.* **97**, 2941 (1993).
15. S. A. Langer, R. E. Goldstein, D. P. Jackson, *Phys. Rev. A* **46**, 4894 (1992).
16. D. P. Jackson *et al.*, unpublished data.
17. The experimental apparatus consisted of a Hele-Shaw cell constructed from two plates of optically flat glass, each 5.78 ± 0.01 mm thick, and separated by a rubber gasket with thicknesses of 1.94 ± 0.01 mm, creating a circular working volume of radius 5.8 cm. The ferrofluid was placed in the center of this volume and surrounded by a dilute solution of surfactant (Tween) in water. The ferrofluid (EMG 901) was obtained from Ferrofluidics (Nashua, NH) with a saturation magnetization of 600 gauss and a viscosity of 10 cp. Once filled, the cell was placed in a water-cooled Helmholtz coil with an outer radius of 18.0 cm. and bore radius of 7.9 cm., whose field uniformity was ± 5 percent from bore center to periphery. The time course of the magnetic field was controlled by a PCL-818 digital to analog converter card and software written for this purpose, and the intrinsic response time of the apparatus was less than 0.1 second. Videotaped images were obtained with a Sony XC-39 CCD video camera collinear with the bore of the Helmholtz coil, and controlled by an NEC PC-VCR (PV-S98A). Recorded images were digitized and processed with edge-detection software.
18. R. E. Rosensweig, M. Zahn, R. Shumovich, *J. Magnetism Magnetic Mater.* **39**, 127 (1983).
19. There are also indications of an important role played by a ferrofluid-glass wetting phenomenon in that two successive patterns often have strong similarities, suggesting the presence of a thin film on the glass surface which biases the arm evolution. This effect can be reduced significantly by manipulating the ferrofluid drop back and forth across the glass prior to the field quench.
20. The magnetization is most uniform for highly regular shapes like the initial condition, which closely approximates an oblate ellipsoid, a shape for which the demagnetizing field is uniform. For highly branched patterns this approximation breaks down as fringing fields come to dominate.
21. Our calculation differs from the important work of D. J. Keller, J. P. Korb, H. McConnell, [*J. Phys. Chem.* **91**, 6417 (1987)], in which the cutoff was added by hand.
22. G. K. Batchelor, *An Introduction to Fluid Dynamics* (Cambridge Univ. Press, Cambridge, 1967), pp. 222–224.
23. For a related hydrodynamic calculation, see H. M. McConnell, *J. Phys. Chem.* **96**, 3167 (1992).
24. See, for example, D. Bensimon, L. P. Kadanoff, S. Liang, B. I. Shraiman, C. Tang, *Rev. Mod. Phys.* **58**, 977 (1986).
25. D. Weaire and N. Rivier, *Contemp. Phys.* **25**, 59 (1984).
26. We thank N. P. Ong, M. Shelley, M. Seul, and R. Rosensweig for their long-standing interest and advice; P. W. Anderson, R. H. Austin, S. M. Gruner, H. M. McConnell, and A. O. Cebers for important discussions; and K. D. Bonin and M. Kadar-Kallin for experimental assistance at an early stage of this work. Funded in part by National Science Foundation grant CHE91-06240, a Department of Energy Graduate Fellowship (A.J.D.), the Alfred P. Sloan Foundation (R.E.G), and the NSERC of Canada (S.A.L.).

6 May 1993; accepted 17 July 1993